GEOPHYSICAL RESEARCH LETTERS, VOL. 35, L24204, doi:10.1029/2008GL036149, 2008

Enceladus: An estimate of heat flux and lithospheric thickness from flexurally supported topography

Bernd Giese,[1] Roland Wagner,[1] Hauke Hussmann,[1] Gerhard Neukum,[2] Jason Perry,[3] Paul Helfenstein,[4] and Peter C. Thomas[4]

Received 26 September 2008; revised 14 November 2008; accepted 14 November 2008; published 30 December 2008.

[1] We have identified flexural uplift along a rift zone of the Harran Sulci, Enceladus, using Cassini images and stereo-derived topography. On the assumption that the upraised topography is related to a flexed elastic plate, shape modeling yields an effective lithospheric thickness of 0.3 km and, combined with the strength envelope, a mechanical lithospheric thickness of 2.5 km with heat fluxes of 200–270 mW/m^2 at the time of formation. The heat fluxes are comparable to average heat flux values measured in Enceladus' active south polar region, and they are consistent with estimates derived via models of unstable extension of the lithosphere at this location. Surface porosity can reduce the obtained heat fluxes to an estimated minimum of 45–60 mW/m^2. Crater-size frequency counts fix the time of formation (from present-day) of the rift zone at either $3.5^{+0.1}_{-0.4}$ Ga (assuming an asteroid-type impact chronology) or $0.45^{+1.1}_{-0.3}$ Ga (assuming a comet-type impact chronology). **Citation:** Giese, B., R. Wagner, H. Hussmann, G. Neukum, J. Perry, P. Helfenstein, and P. C. Thomas (2008), Enceladus: An estimate of heat flux and lithospheric thickness from flexurally supported topography, *Geophys. Res. Lett.*, *35*, L24204, doi:10.1029/2008GL036149.

1. Introduction

[2] Voyager- and Cassini observations have revealed a complex geologic history of Enceladus [*Smith et al.*, 1982; *Porco et al.*, 2006]. Different from its sibling Mimas, which exhibits an ancient surface, most of Enceladus has been resurfaced, and its south polar region is currently active, showing anomalous high temperatures and erupting plumes [*Spencer et al.*, 2006; *Porco et al.*, 2006]. Thermal models can help unfold important details of this history [e.g., *Schubert et al.*, 2007; *Tobie et al.*, 2008]; however, such models are hard to constrain primarily because Enceladus' internal composition and structure are poorly understood, and its orbital eccentricity, which governs the strength of tidal heating, may have been higher in the past [*Roberts and Nimmo*, 2008].

[3] In this paper, we present new constraints for thermal models of Enceladus. Using recent Cassini imaging data, we derive a local heat flux that leads to specific implications for the past regional thermal state. The heat flux is estimated from flexurally supported topography, and the time to which the estimate applies is determined by crater size-frequency counts.

2. Observations

[4] We study a region of the Harran Sulci located at the transition from Diyar Planitia to older cratered plains (~3°N, 130°E) (Figure 1). In this region Enceladus exhibits an 11 km wide N–S trending half-graben structure that, as stereo-derived topography reveals, has an elevated western flanking ridge (Figures 1 and 2). The ridge rises up to ~1 km above the local surroundings and is interpreted to have formed by flexural uplift in response to unloading caused by extension, as sketched in Figure 1. Towards the north, the ridge degrades into sub-parallel km-scale ridges and troughs and it becomes broader and shallower (Figure 2). This morphology and the young age (Figure 1) suggest post-formational extension in this part of the ridge. Consequently, we have exempted it from our modeling. The cumulative extension [*Giese et al.*, 2007] across the half-graben is 1.1 km, and the associated strain is 11.1%.

3. Theory and Methods

[5] The method we apply to derive the heat flux is elaborated in a previous paper [*Giese et al.*, 2007]; here we give just a short outline. We treat the lithosphere as a cracked elastic plate [*Turcotte and Schubert*, 2002] and first determine the flexural parameter α by modeling the shape of the plate. α is related to the effective thickness T_e of the elastic plate by

$$\alpha = \left(\frac{E \cdot T_e^3}{3 \cdot (1 - \nu^2) \cdot \Delta\rho \cdot g} \right)^{\frac{1}{4}}, \qquad (1)$$

where E is the Young's modulus, ν is the Poisson's ratio of the material, g is the gravitational acceleration, and $\Delta\rho$ is the density contrast between the lithosphere and the material above. T_e is then related to the strength envelope of the lithosphere following the formalism described by *McNutt* [1984]. This yields the heat flux F and also the mechanical thickness T_m of the lithosphere. In detail, we solve the equation

$$T_e = \left\{ \frac{12 \cdot (1 - \nu^2)}{E \cdot K_{\max}} \int_0^{T_m} \sigma(z) \cdot (z - z_n) dz \right\}^{1/3}, \qquad (2)$$

where $\sigma(z)$ is the differential stress at depth z (Section 4), $K_{\max}$ is the maximum curvature of the plate, and z_n is a

[1] Institute of Planetary Research, DLR, Berlin, Germany.
[2] Department of Earth Sciences, Freie Universität Berlin, Berlin, Germany.
[3] Department of Planetary Sciences, University of Arizona, Tucson, Arizona, USA.
[4] Center for Radiophysics and Space Research, Cornell University, Ithaca, New York, USA.

0094-8276/08/2008GL036149$05.00

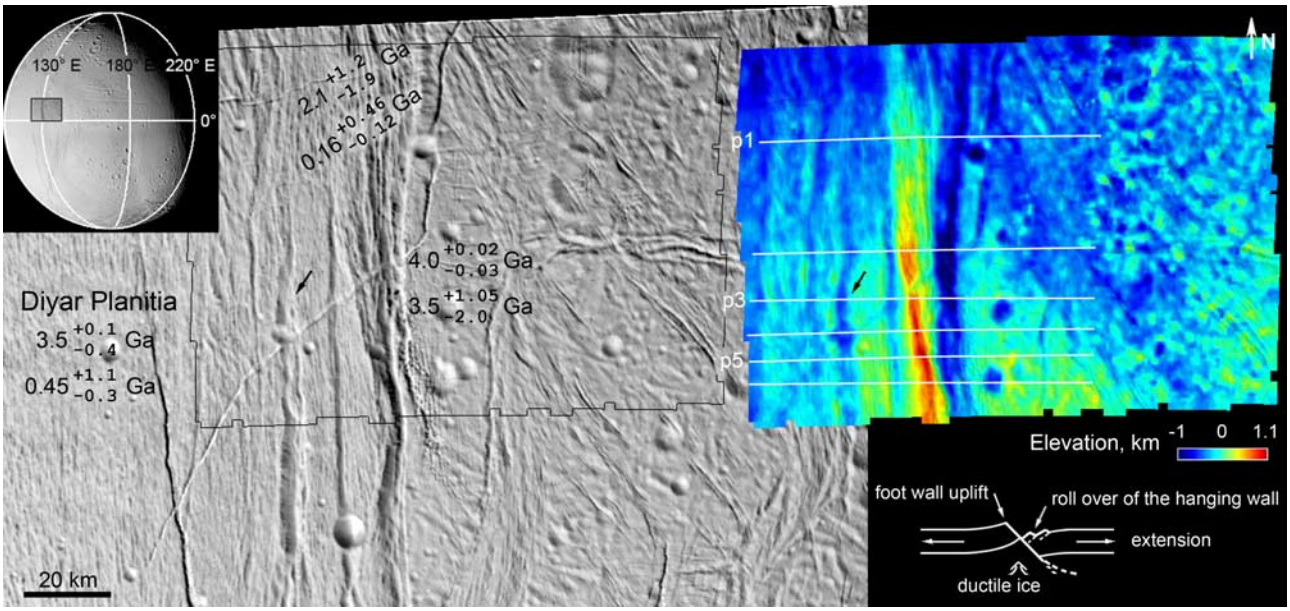

Figure 1. Overview image showing the study area (highlighted) within the Harran Sulci (top left inset). Cut-out of Cassini frame N1489048222 (159 m/pxl) (center). Numbers shown denote ages of different geological units derived from an asteroid-based (upper row) and comet-based (bottom row) impact chronology model, respectively (Section 6). The black contour line marks the location of a Digital Elevation Model (DEM) in this area (top right inset) that was derived from N1489048222 and N1489049936 (86 m/pxl) using methods of photogrammetry [*Giese et al.*, 1998]. The DEM measures local relief only and resolves features with horizontal dimensions of 0.5–1 km at vertical accuracies of 150–300 m. Cross-sectional sketch showing how the ridge is thought to have formed (bottom right inset).

depth fixed by the condition that the stress profile integrates to zero. A selected stress profile is shown in Figure 3.

4. Constitutive Relations and Strength Parameters

[6] The surface of Enceladus is covered in almost pure water ice [*Ostro et al.*, 2006; *Jaumann et al.*, 2008], and we assume that this also holds up to depths of some kilometers. For the stresses in the brittle zone we adopt the relations given by *Beeman et al.* [1988] with a slope of 0.69 and an intercept equal to zero. The ductile ice strengths are calculated from equation [*Goldsby and Kohlstedt*, 2001]

$$\dot{\varepsilon} = \left(\frac{1}{\dot{\varepsilon}_{gbs}} + \frac{1}{\dot{\varepsilon}_{basal}}\right)^{-1} + \dot{\varepsilon}_{disl} + \dot{\varepsilon}_{diff} \tag{3}$$

with strain rates $\dot{\varepsilon}_i$ specific to grain boundary sliding (*gbs*), dislocation creep (*disl*), basal or easy slip (*basal*), and volume diffusion (*diff*). Their general form can be written as [*Goldsby and Kohlstedt*, 2001; *Ranalli*, 1995]

$$\dot{\varepsilon}_i = \left(\frac{\sqrt{3}}{2}\right)^{n_i+1} \cdot A_i \cdot \left(\frac{1}{d}\right)^{m_i} \cdot \sigma^{n_i} \cdot \exp\left\{-\frac{Q_i}{R \cdot T}\right\}, \tag{4}$$

where d is the grain size, R is the gas constant, T is the temperature, and Q is the activation energy. Q_i, A_i, m_i, and n_i are process-dependent parameters given in Table 1. For the temperature of the ductile layer we adopt a conductive profile that takes into account porosity effects of the brittle ice above. We use (see Appendix A)

$$T(z) = T_s \cdot \exp\left\{\frac{F}{567} \cdot (z - d_b \cdot [1 + 1/p - \exp(p)/p])\right\}, \tag{5}$$

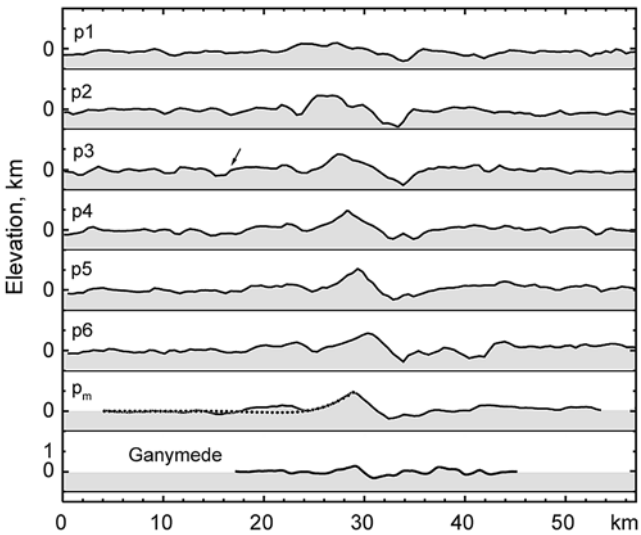

Figure 2. Profiles showing the morphology of the half-graben (for profiles' location see Figure 1). P_m is the mean of p4–p6 and finally used in the modeling. The dotted line represents the model flexural profile (Section 5). The arrow in p3 points to a feature with simple graben morphology (see also Figure 1). Bottom profile shows the relief of a half-graben structure on Ganymede [*Giese et al.*, 2001]. Vertical exaggeration is 2.

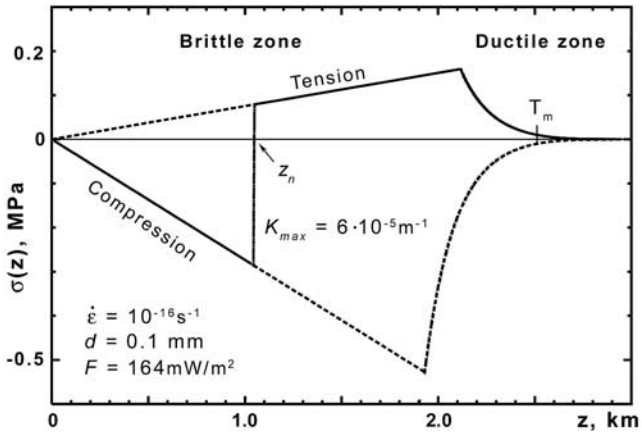

Figure 3. Selected stress profile (solid line) used in equation (2). Because of the exponential drop of the stress in the ductile zone the integrations are effectively stopped at depth T_m where $\sigma(z)$ falls below 0.01 MPa. The stress changes continuously from compressional to extensional at the neutral fiber z_n of the bending plate. Brittle and ductile strengths relations are given in Section 4.

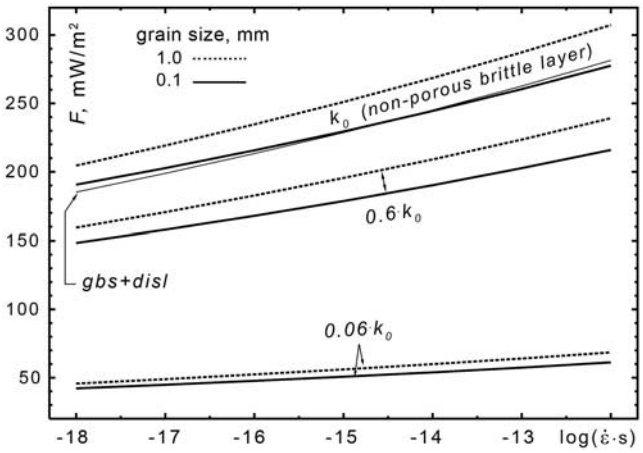

Figure 4. Heat flux as a function of strain rate at different grain sizes and degree of porosity of the brittle layer. For porous brittle layers, the heat fluxes decrease as the surface conductivity decreases from 0.6 k_0 to 0.06 k_0. The thin solid line (gbs + disl) represents the heat flux if ductile creep is accomplished by grain boundary sliding and dislocation creep only (Section 4).

where T_s is the surface temperature, F is the heat flux [mW/m^2], z is the depth [km], d_b is the thickness of the brittle layer [km], and p is a number that models the drop of thermal conductivity towards the surface due to porosity. Specifically, the surface conductivity is $k_0\exp(-p)$ and the conductivity reaches the non-porous value k_0 at the base of the brittle layer.

[7] Throughout the calculations, we adopt $\Delta\rho = 920$ kg/m^3, g = 0.113 m/s^2 [*Thomas et al.*, 2007], $\nu = 0.33$, E = 1 GPa, and T_s = 65 K, which corresponds to the diurnal average surface temperature currently measured at the equator [*Spencer et al.*, 2006].

5. Results

[8] As observational data in the modeling we use a mean profile (Figure 2). The best fit is obtained with α = 3.14 km corresponding to T_e = 0.3 km (dotted line). The maximum curvature of the plate is $K_{\max} = 6 \cdot 10^{-5}$ m^{-1}. Resulting heat fluxes predicted by equation (2) are shown in Figure 4. For non-porous ice and geological strain rates of 10^{-17}–10^{-14} s^{-1} the heat fluxes are in the range of 200–270 mW/m^2. The associated mechanical lithospheric thickness is T_m = 2.5 km for all strain rates and grain sizes considered. Varying Young's modulus by an order of magnitude changes the solution by less than 1 mW/m^2. The dependence on the adopted stress limit (see Figure 3) is also weak. Halving this value raises T_m by less than 100 m and F by less than 1 mW/m^2.

[9] Porosity of the brittle layer lowers the obtained heat fluxes. For an adopted maximum porous conductivity of $0.6 \cdot k_0$ at the surface the heat flux decreases by ~21%, and for a minimum of $0.06 \cdot k_0$ the decrease is by ~77% (Figure 4).

[10] Grain boundary sliding and dislocation creep are the dominant creep processes in determining the heat fluxes here (Figure 4).

Table 1. Rheologic Parameters Used in the Calculations[a]

Creep Process	n	m	Q [kJ/mol]	A [MPa^{-n} m^m s^{-1}]
grain boundary sliding	1.8	1.4	49	3.9×10^{-3}
basal or easy slip	2.4	0	60	5.5×10^{7}
dislocation creep	4	0	60	4.0×10^{5}
volume diffusion	1	2	59.4	[b]

[a]After *Goldsby and Kohlstedt* [2001].

[b]For volume diffusion, A depends on temperature given by $A = \frac{42 \cdot V_m \cdot D_{0,\nu}}{R \cdot T}$ with $V_m = 1.97 \cdot 10^{-5}$ m^3 · mol^{-1}, $D_{0,\nu} = 9.1 \cdot 10^{-4}$ m^2 · s^{-1}.

6. Ages

[11] The flanking ridge of the half-graben is stratigraphically tied to Diyar Planitia (Figure 1). While this suggests that both are similar age, a younger age for the half-graben cannot be excluded. To determine ages we performed crater size-frequency measurements. Absolute ages (Figure 1) are derived from two different impact chronology models: the lunar-like model, which is based on impacts preferentially by asteroids [*Neukum*, 1985], and the model by *Zahnle et al.* [2003] (here we only consider the relevant Case A discussed by the authors), which is based on comets as major impactors. The crater counts were carried out in images with resolutions of 24–188 m/pxl taken during Cassini's 4th orbit (see auxiliary material).[1]

7. Discussion and Conclusions

[12] The best fit model profile shown in Figure 2 ignores an apparent horst to the west of the ridge with the implicit understanding that its formation was superimposed on the formation of the flanking ridge. Otherwise T_e would increase to 0.75 km (and T_m to 3.6 km) and the obtained heat

[1]Auxiliary materials are available in the HTML. doi:10.1029/2008GL036149.

fluxes would decrease by about 30% which, however, is less compared with uncertainties related to the porosity structure.

[13] Measurements of Enceladus' thermal inertia [*Spencer et al.*, 2006] imply a highly unconsolidated surface up to depths of ~1 cm. The effect of a very low-density insulating surface layer can be taken into account in our model via a higher surface temperature T_s, which (in our model) actually is a temperature at depths where no more diurnal variations occur. Using T_s = 80 K rather than 65 K (Section 4) yields heat fluxes by ~20% lower.

[14] Prevailing strain rates during the formation of the half-graben are unknown but a plausible range can be identified on the basis of the measured extension [*Giese et al.*, 2007]. Assuming that the time span of formation was not shorter than a few 0.1 Ma and not longer than a few 100 Ma, the range of strain rates must then be limited to $\sim 10^{-17}$–10^{-14} s^{-1}.

[15] The derived heat fluxes and the mechanical lithospheric thickness characterize the local thermal state associated with the formation of the half-graben, but probably, this state applies to the whole region of Diyar Planitia (Section 6). However, we note that warm ice welling up in the rift zone in response to extensional unloading could have enhanced the heat flux there. The intrusion of warm ice is fundamentally presumed to have caused the uplifted rift flank, but its possible contribution to the obtained heat flux remains open.

[16] If near-surface porosity is neglected the obtained heat fluxes of 200–270 mW/m^2 give a good match to those derived via models of unstable extension of the lithosphere. In the framework of that model *Bland et al.* [2007] derived heat fluxes of 110–220 mW/m^2 in Diyar Planitia. Moreover, our heat fluxes are as high as average heat fluxes of 250 mW/m^2 measured in Enceladus' south polar region [*Spencer et al.*, 2006]. This suggests high thermal activity already earlier in its history. However, the effects of near-surface porosity may be important on Enceladus. This is expected from its low gravity and associated low overburden pressure and predicted by experimental work [*Durham et al.*, 2005]. On the other hand, significant heating at depth, which is plausible in view of the obtained high heat fluxes and the high predicted interior temperatures [*Matson et al.*, 2007], may have removed porosity by viscous creep. The true porosity structure is likely complex and is unknown. Thus, in modeling the conductivity (Appendix A) we consider the warmer ductile ice to be non-porous, and for the brittle layer we have chosen a simple 1-parameter ansatz that provides a reasonable order-of-magnitude estimate of porosity effects on the heat fluxes. The adopted limits of porous conductivity are those considered for Kuiper Belt objects [*McKinnon*, 2002]. At the highest adopted porosity the obtained heat fluxes are reduced to 45–60 mW/m^2, which demonstrates the significance of porosity effects here and, at the same time, stresses the importance of knowing the porosity structure in thermal modeling.

[17] An independent estimate of lithospheric thickness can be obtained from an apparent simple graben structure which has formed in Diyar Planitia (Figure 2). Simple grabens are bounded by normal faults that converge at the brittle-ductile transition and thus are probes of the lithosphere as well [*Golombek and Banerdt*, 1986]. From the measured graben width of 2.5–3.5 km and fault dip (assumed to be 60°) the brittle layer thickness results in 2–3 km consistent with the brittle-ductile transition depth of 2.1 km inferred from Figure 3.

[18] Differential stresses at the brittle-ductile transition are ~0.15 MPa (Figure 3). Such stresses are required to cause frictional sliding there. Diurnal tidal stresses [*Hurford et al.*, 2007] are of the same order and thus could have caused frictional tidal heating in Enceladus' brittle zone.

[19] Rift zones on Jupiter's satellite Ganymede exhibit relief of typically some hundred meters [*Nimmo et al.*, 2002; *Nimmo and Pappalardo*, 2004] (an example with flank-uplift of 280 m is shown in Figure 2). This is markedly less relief than obtained for Enceladus (940 m) and may be related to the higher stresses on Ganymede to initiate frictional sliding. Frictional sliding forces scale with gravity, which, however, is 12 times higher on Ganymede than on Enceladus.

Appendix A

[20] Here we derive a temperature profile of the ductile (assumed to be non-porous) ice at given heat flux F if the brittle ice above is porous. Generally, the heat flux is related to temperature via $F = k \cdot \frac{\partial T}{\partial z}$, where k is the thermal conductivity. For the ductile ice we apply the thermal conductivity of pure water ice as given by *Klinger* [1980], $k_0 = 567/T$, and for the brittle porous part we adopt a simple 1-parameter ansatz in the form $k_0 \cdot \exp\{-p \cdot (1-z/d_b)\}$, where d_b is the brittle layer thickness, and p is a positive number that models the degree of porosity. Solving these equations for each part and imposing the condition that the temperature must be continuous at the transition the ductile ice temperature profile is given by

$$T(z) = T_s \cdot \exp\left\{\frac{F}{567} \cdot (z - d_b \cdot [1 + 1/p - \exp(p)/p])\right\}.$$

[21] **Acknowledgment.** The authors would like to thank Ernst Hauber and the reviewers for helpful comments.

References

Beeman, M., W. B. Durham, and S. H. Kirby (1988), Friction of ice, *J. Geophys. Res.*, *93*, 7625–7633.

Bland, M. T., R. A. Beyer, and A. P. Showman (2007), Unstable extension of Enceladus' lithosphere, *Icarus*, *192*, 92–105, doi:10.1016/j.icarus.2007.06.011.

Durham, W. B., W. B. McKinnon, and L. A. Stern (2005), Cold compaction of water ice, *Geophys. Res. Lett.*, *32*, L18202, doi:10.1029/2005GL023484.

Giese, B., J. Oberst, T. Roatsch, G. Neukum, J. W. Head, and R. T. Pappalardo (1998), The local topography of Uruk Sulcus and Galileo Regio obtained from stereo images, *Icarus*, *135*, 303–316.

Giese, B., R. Wagner, G. Neukum, R. T. Pappalordo, J. W. Head III, and The Galileo Imaging Team (2001), The topography of dark/bright terrain on Ganymede, *Lunar Planet. Sci.*, *XXXII*, Abstract 1751.

Giese, B., R. Wagner, G. Neukum, P. Helfenstein, and P. C. Thomas (2007), Tethys: Lithospheric thickness and heat flux from flexurally supported topography at Ithaca Chasma, *Geophys. Res. Lett.*, *34*, L21203, doi:10.1029/2007GL031467.

Goldsby, D. L., and D. L. Kohlstedt (2001), Superplastic deformation of ice: Experimental observations, *J. Geophys. Res.*, *106*, 11,017–11,030.

Golombek, M. P., and W. B. Banerdt (1986), Early thermal profiles and lithospheric strength of Ganymede from extensional tectonic features, *Icarus*, *68*, 252–265.

Hurford, T. A., P. Helfenstein, G. V. Hoppa, R. Greenberg, and B. G. Bills (2007), Eruptions arising from tidally controlled periodic openings of rifts on Enceladus, *Nature*, *447*, 292–294, doi:10.1038/nature05821.

Jaumann, R., et al. (2008), Distribution of icy particles across Enceladus' surface as derived from Cassini-VIMS measurements, *Icarus*, *193*, 407–419, doi:10.1016/j.icarus.2007.09.013.

Klinger, J. (1980), Influence of a phase transition of ice on the heat and mass balance of comets, *Science*, *209*, 271–272.

Matson, D. L., J. C. Castillo, J. Lunine, and T. V. Johnson (2007), Enceladus' plume: Compositional evidence for a hot interior, *Icarus*, *187*, 569–573, doi:10.1016/j.icarus.2006.10.016.

McKinnon, W. B. (2002), On the initial thermal evolution of Kuiper belt objects, in *Proceedings of Asteroids, Comets, Meteors*, *ACM 2002*, edited by B. Warmbein, *Eur. Space Agency Spec. Publ.*, *500*, 29–38.

McNutt, M. K. (1984), Lithospheric flexure and thermal anomalies, *J. Geophys. Res.*, *89*, 11,180–11,194.

Neukum, G. (1985), Cratering records of the satellites of Jupiter and Saturn, *Adv. Space Res.*, *5*, 107–116.

Nimmo, F., and R. T. Pappalardo (2004), Furrow flexure and ancient heat flux on Ganymede, *Geophys. Res. Lett.*, *31*, L19701, doi:10.1029/2004GL020763.

Nimmo, F., R. T. Pappalardo, and B. Giese (2002), Effective elastic thickness and heat flux estimates on Ganymede, *Geophys. Res. Lett.*, *29*(7), 1158, doi:10.1029/2001GL013976.

Ostro, S., et al. (2006), Cassini RADAR observations of Enceladus, Tethys, Dione, Rhea, Iapetus, Hyperion, and Phoebe, *Icarus*, *183*, 479–490, doi:10.1016/j.icarus.2006.02.019.

Porco, C. C., et al. (2006), Cassini observes the active south pole of Enceladus, *Science*, *311*, 1393–1401.

Ranalli, G. (1995), *Rheology of the Earth*, 2nd ed., Chapman and Hall, London.

Roberts, J. H., and F. Nimmo (2008), Tidal heating and the long-term stability of a subsurface ocean on Enceladus, *Icarus*, *194*, 675–689, doi:10.1016/j.icarus.2007.11.010.

Schubert, G., J. D. Anderson, B. J. Travis, and J. Palguta (2007), Enceladus: Present internal structure and differentiation by early and long-term radiogenic heating, *Icarus*, *188*, 345–355, doi:10.1016/j.icarus.2006.12.012.

Smith, B. A., et al. (1982), A new look at the Saturn system: The Voyager 2 images, *Science*, *215*, 504–537.

Spencer, J. R., et al. (2006), Cassini encounters Enceladus: Background and the discovery of a south polar hot spot, *Science*, *311*, 1401–1405.

Thomas, P. C., et al. (2007), Shapes of the Saturnian icy satellites and their significance, *Icarus*, *190*, 573–584, doi:10.1016/j.icarus.2007.03.012.

Tobie, G., O. Cadek, and C. Sotin (2008), Solid tidal friction above a liquid water reservoir as the origin of the south pole hotspot on Enceladus, *Icarus*, *196*, 642–652, doi:10.1016/j.icarus.2008.03.008.

Turcotte, D. L., and G. Schubert (2002), *Geodynamics*, 2nd ed., Cambridge Univ. Press, Cambridge, U.K.

Zahnle, K., P. Schenk, H. Levison, and L. Dones (2003), Cratering rates in the outer solar system, *Icarus*, *163*, 263–289.

B. Giese, H. Hussmann, and R. Wagner, Institute of Planetary Research, DLR, Rutherfordstraße 2, D-12489 Berlin, Germany. (bernd.giese@dlr.de)

P. Helfenstein and P. C. Thomas, Center for Radiophysics and Space Research, Cornell University, Ithaca, NY 14853, USA.

G. Neukum, Department of Earth Sciences, Freie Universität Berlin, D-12249 Berlin, Germany.

J. Perry, Department of Planetary Sciences, University of Arizona, Tucson, AZ 85721, USA.